1D DIFFUSION MODEL FOR MODERATE PRESSURE H_2 PLASMAS USED FOR DIAMOND FILMS DEPOSITION

K. Hassouni*, S. Farhat*, C. D. Scott**, A. Gicquel*

* Laboratoire d'Ingéniérie des Matériaux et des Hautes Pressions (LIMHP) CNRS-Université Paris XIII, Av. J. B. Clément, Villetaneuse 93430, France
** NASA Johnson Space Center, Houston, TX 77058 USA.

Abstract

A one dimensional model for thermochemically non equilibrium diffusive flows was used to investigate the H_2 plasma obtained in a diamond deposition bell jar reactor. The comparison of the calculated results with experimental measurements showed that the gas and H_2 vibration temperatures are well predicted by the model. For an H-atom recombination coefficient of 0.1, the calculated axial profile of H-atom shows a boundary layer thickness comparable to that of the experimental profile even if the calculated values of $[H]/[H]_{bulk}$ are substentially higher than those determined by actinometry measurements.

I. Introduction

In the last few years, microwave H_2/CH_4 plasmas, obtained under moderate pressure (10 mbar <P < 100 mbar) discharge conditions have prooved their efficiency for deposition of high quality diamond films [1]. However, the improvement and the optimization of diamond MPACVD processes requires a better understanding of the chemistry and the transport in the plasma flow. The investigation of H_2/CH_4 diamond deposition plasmas requires at first a good description of pure H_2 plasma obtained under diamond deposition discharge conditions [2]. We report here results of plasma diffusion simulations carried out by solving the transport equations resultiong from an H_2 plasma model established by Scott, et al. In this reactor the deposition substrate is positioned in a stagnation point configuration and the discharge takes place in a hemispherical volume located just above the substrate (fig. 1). Although convection might occur in typical deposition experiments conditions, the Peclet number is very low and the convection fluxes should be neglected compared to the diffusion fluxes. The investigated plasma region, in this work, is one dimensional and located on the plasma axis where all the radial gradients are zero (fig. 2). As a consequence, the equations describing the plasma diffusion are expressed in one dimensional geometry.

II. The transport model

II. 1. Model assumptions

Under diamond deposition discharge conditions, the heavy particles translation-rotation energy, H_2 vibration energy and electrons translation energy modes in an H_2 plasma are not in equilibrium and the major chemical species are H_2, H, H^+, H_2^+, H_3^+, H^- and e^- [3]. The transport of these chemical species and energy modes are coupled through the species chemical production rates which strongly depend on the different energy modes. As a consequence, the model presented here results in a description of the plasma by 7 species transport equations coupled to three energy transport equations. It assumes that the distribution functions of the three energy modes are Maxwell-Boltzmann with three different temperatures (Tg, Tv and Te).

II. 2. Model Equations

The set of plasma mass and energy transport governing equations are summarized in the following subsections.

II. 2. .1. Species continuity equations

$$-\frac{d}{dz}\left[\rho.D_s\frac{dx_s}{dz}\right]=W_s \quad (s=1,7) \tag{1}$$

ρ is the plasma total mass density. x_s, D_s and W_s are the molar fraction, the diffusion coefficient and the chemical production rate of the species 's'. W_s was estimated from an H_2 plasma kinetic model reported in reference [3]. However, the rate constants used in this model were recently improved using the collisions cross sections recommended by Phelps [4].

II. 2. 2. H_2 vibration energy equation

$$-\frac{d}{dz}\left[\lambda_v.\frac{dT_v}{dz}\right]-\frac{d}{dz}\left[\rho.D_{H2}.E_{v\text{-}H2}\frac{dx_{H2}}{dz}\right]=-Q_{v\text{-}e}-Q_{v\text{-}t} \tag{2}$$

The two derivatives appearing in the left hand side (LHS) of equation (2) are flux terms corresponding to the vibration energy conduction and to the diffusion of vibrationaly excited H_2. The source terms $Q_{v\text{-}e}$ and $Q_{v\text{-}t}$ correspond to the rates of energy transfered from H_2 vibrational mode to the electron kinetic mode and to the heavy particles translation-rotation mode. λ_v is the vibration energy conduction coefficient and $E_{v\text{-}H2}$ is the H_2 vibrational energy per unit mass.

II. 2. 3. Electron energy equation

$$-\frac{d}{dz}\left[\lambda_e.\frac{dT_e}{dz}\right]-\frac{d}{dz}\left[\rho.D_e.h_e\frac{dx_e}{dz}\right]=PMW-Q_{e\text{-}v}-Q_{e\text{-}t}-Q_{e\text{-}chem} \tag{3}$$

The LHS of this equation accounts for the energy fluxes due to conduction transport and electron diffusion. The source terms, $Q_{e\text{-}v}$ and $Q_{e\text{-}t}$, account for the energy transfer from the electron energy mode to the H_2 vibration energy mode and heavy particles translation-rotation mode. $Q_{e\text{-}chem}$ is the rate of energy loss by chemical processes activation (dissociation of H_2 and ionization of H_2 and H). PMW is the microwave power density absorbed by the electrons. The spatial distribution of PMW is a model

input parameter whose choice will be discussed in the next section. λ_e is the electron energy mode conduction coefficient and h_e is the electron enthalpy.

II. 2. 4. Total energy equation

$$-\frac{d}{dz}\left[\lambda_e \cdot \frac{dT_e}{dz} + \lambda_v \cdot \frac{dT_v}{dz} + \lambda_{t\text{-}r} \cdot \frac{dT_g}{dz}\right] - \sum_s \frac{d}{dz}\left[\rho . D_s . h_s \frac{dx_s}{dz}\right] = PMW - Q_{rad} \qquad (4)$$

The fluxes term appearing in the LHS of equation (4) correspond to the conduction of the three energy modes and to the diffusion of the enthalpic species. The source terms correspond to the microwave power absorbed by the electrons, PMW, and to the energy loss by radiation, Q_{rad}. $\lambda_{t\text{-}r}$ is the translation-rotation mode conduction coefficient and h_s the 's' species massic enthalpy. The expressions of the transport coefficients and energy transfer source terms may be found in reference [2].

III. Absorbed microwave power density and boundary conditions

III. 1. macroscopic power balance

At the steady state regime, the microwave power absorbed by the plasma is transferred to the substrate and to the reactor wall. The energy flux at the substrate center has been estimated from Coherent Antistokes Raman Spectroscopy measurements (CARS) previously carried out on the studied reactor[1]. For the investigated discharge conditions, power density of 9 W/cm^3, this flux has been estimated to 20 W/cm^2. Assuming that this density is approximatly constant over all the substrate section, among the 600W input power, 390 W is transfered to the substrate surface, the reminder being transferred to the reactor walls and gas effluents. Since the present model is one dimensional and does not take the energy transfered from the plasma to the reactor walls into account, the plasma behavior in the simulation domain of fig. 2 is described by considering that the plasma volume and the deposition substrate are isolated from the reactor walls and that the effective absorbed microwave power is equal to the power transferred to the substrate.

III. 2. Spatial distribution of the absorbed microwave power

The solution of the 1D transport equations requires the knowledge of the axial profile of the absorbed microwave power density which appears in the electron energy and the total energy equations. The axial distribution of the absorbed microwave power density is assumed to be the solution of the one dimensional wave equation where the wave is assumed to be injected at the top of the reactor and reflected back on a plate at the end of the reactor. The radial profile was assumed to be similar to the axial one. We have also assumed that the plasma electrical permittivivity is constant over all the plasma volume. The absorbed power distribution is then given by the following relation :

$$PMW(z,r) = Po \cdot \cos^2\left(\frac{2\pi(z-z_0)}{\lambda}\right) \cdot \cos^2\left(\frac{2\pi r}{\sqrt{\lambda^2/16 - z^2}}\right) \quad (5)$$

Where λ is the wave length of the high frequency electric field (λ=12 cm). z_0 is the position of the maximum power density which was set equal to zero in the present simulation. Po was determined from the following energy balance :

$$P_{total} = \iint_{hemisphere} PMW(z,r)\ 2\pi.r.dr)).dz \quad (6)$$

Where P_{total} is the total absorbed power.

III. 3. Boundary conditions

The solution of the transport equations (1)-(4) requires the specification of the species concentrations and of the temperatures boundary conditions at the computation domain inlet and at the substrate surface. Since, in this model, the plasma hemisphere and the substrate are considered to be isolated from the remainder of the reactor, the boundary conditions at the inlet $z=z_I$ are derived by setting to zero all the gradients :

$$\left.\frac{d\phi}{dz}\right|_{subst} = 0 \ ; \ \phi = x_s,\ T_g,\ T_e \text{ and } T_v \ \ (s=1,\ldots,7) \quad (8)$$

At the substrate surface, the gas temperatures is set equal to the substrate surface temperature, the H_2 vibration temperature is estimated from the value measured by CARS measurements at 0.5 mm from the surface. The accommodation of the electrons energy at the substrate is very weak [2], and zero gradient of T_e may be assumed at the substrate surface. The boundary conditions for the chemical species were derived from the surface reactions mechanism reported by Scott[2]. The resulting boundary conditions may be written :

$$T_g|_{subst} = T_{g\text{-}exp} \ ; \ T_v|_{subst} = T_{v\text{-}exp} \ ; \ \left.\frac{dT_e}{dz}\right|_{subst} = 0 \text{ and } \left.\frac{dx_s}{dz}\right|_{subst} = -\frac{W_{s\text{-}subst}}{\rho.D_s} \quad (9)$$

$W_{s\text{-}subst}$ is the rate of chemical production of the species 's' at the substrate by surface reaction. It was derived assuming a total catalytic recombination for the ions (γ_{ions}=1) and a partial recombination for H-atom ($\gamma_H = 0.1$)

IV. Results and discussions

For the absorbed microwave power density axial profile presented in fig. 3, the calculated electron temperature (fig. 3) reaches 18000 K in the plasma bulk (0.5cm<z<2cm) and slightly increases in the vicinity of the substrate surface (0<z<0.3 cm).

The computed gas and H_2 vibration temperatures are nearly in equilibrium over all the plasma, the calculated axial profiles are in good agreement with those determined by CARS [1] (Tg_{exp}-Tg_{model} < 100 K). They show a sharp decrease of T_g from a value of 2000 K in the plasma bulk (z>2cm) to 1100 K at the substrate surface (fig. 4). The value of the thermal boundary layer thickness obtained from both the experiment and the model is about 2 cm. For the investigated discharge conditions, the calculated H-

atom molar fraction in the plasma bulk is 4.5 10^{-2}. The calculated axial profile of the normalized H-atom molar fraction : $[H]/[H]_{bulk}$, is given in figure 5, where the experimental profile, obtained from actinometry measurements [1], of this ratio is also presented. The comparison between the measured and calculated profiles shows that the H-atom diffusion boundary layer thickness is well predicted by the model (δ=2 cm). The calculated values of $[H]/[H]_{bulk}$ near the substrate (0.1 cm <z < 1 cm) are however higher than those measured by actinometry.
The major ionic species are the electrons, H_3^+ and H^+ which molar fraction axial distributions are presented in fig. 6. The electron and H_3^+ molar fraction show similar evolution in the plasma, they reach maximum values of 1.8 10^{-5} and 1.2 10^{-5} at 10 mm and 8 mm from the substrate surface. The molar fraction of H^+ ion is nearly constant and is about 5 10^{-6} in the plasma bulk (1cm < z< 3 cm) and decreases for z < 1 cm.
The H_2^+ and H^- ions, even very important for the kinetic modeling of this kind of plasma, has very low molar fractions which are characterized by maximum values of 5.10^{-9} for H_2^+ and 2.10^{-8} for H^-.

V. Conclusions

The one dimensional transport model presented here enables to estimate some key parameters for H_2 plasmas obtained under diamond deposition discharge conditions. The comparison of the model results and some experimental measurements shows that the gas and H_2 vibration temperatures are well predicted by the model. The discrepency between the calculated and measured H-atom molar fraction show that the chemical kinetic modeling of the discharge must be improved by taking the non Maxwellian behavior of the EEDF into account. Finally, the model results are very sensitive to the absorbed microwave power density spatial distributions [6] which strongly depends of the plasma composition. As a consequence, the plasma transport model presented here may be improved by coupling the electric field equations to the transport equations and determining selfconsistently the absorbed microwave power axial profile.

References

[1] A. Gicquel, K. Hassouni, S. Farhat, Y. Breton, C. D. Scott, M. Lefebvre, M. Pealat, Diam. and Rel. Mat. , Vol. 3, n° 4-6, pp 581-586 (1994).
[2] C. D. Scott, S. Farhat, A. Gicquel, K. Hassouni, M. Lefebvre, M. Péalat. AIAA 93-3226, 1993
[3] S. Farhat, K. Hassouni , A. Gicquel. Abstracts of the 12th ESCAMPIG, Vol. 18E, Noordwijkerhout, The Netherland, August 23-26, 1994.
[4] A. V. Phelps, J. Chem. Phys. Ref. data, Vol. 19, n° 3, pp 653-675, 1993.
[5] M. Capitelli, G. Colonna, K. Hassouni and A. Gicquel, Chem. Phys. Lett., 228, pp. 687-694, 1994.
[6] K. Hassouni, S. Farhat, C. D. Scott and A. Gicquel Diamant. To be published in the Proceedings of Applied Diamond Conference, August 21-24, Maryland USA, 1995.

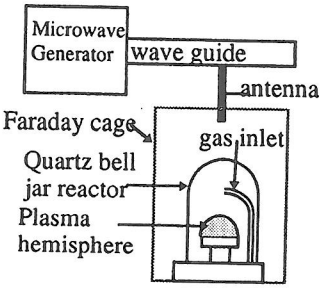

Fig. 1 : Schematic of the deposition setup

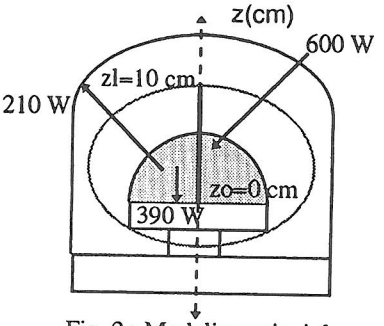

Fig. 2 : Modeling principle

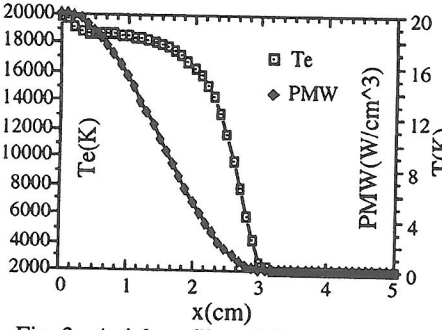

Fig. 3 : Axial profiles of the absorbed microwave power and of the calculated electron temperature

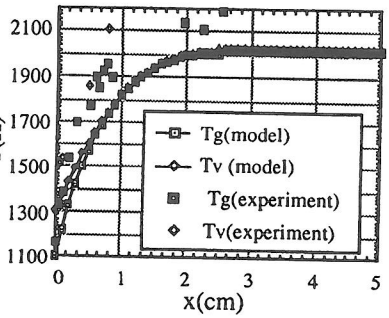

Fig. 4 : Axial profiles of the calculated and measured Tg and Tv

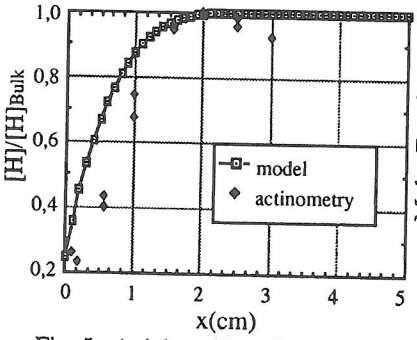

Fig. 5 : Axial profiles of the H-atom molar fraction obtained from the model and measured by actinometry

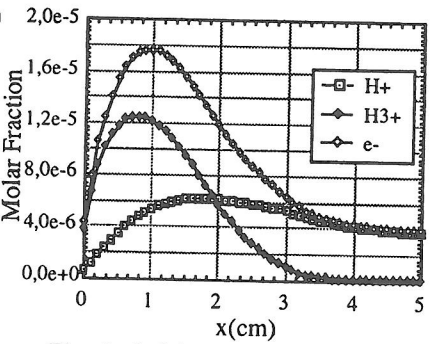

Fig. 6 : Axial profil of the electron, H^+ and H_3^+ molar fractions